

SPH simulations of structures in protoplanetary disks

T.V. Demidova¹, V.P. Grinin^{1,2}

1 - Pulkovo Astronomical Observatory of the Russian Academy of Sciences, Pulkovskoe shosse 65, St. Petersburg, 196140 Russia

2 - S. Petersburg State University, V.V. Sobolev Astronomical Institute, Universitetskii pr. 28, St. Petersburg, 198504 Russia

e-mail:proximal@list.ru

Abstract

The hydrodynamic models of the protoplanetary disk, which perturbed by the embedded low-mass companion, were calculated by our modification of GADGET-2 code. The cases of circular and eccentric orbits which can be coplanar or slightly inclined to the disk midplane were considered. The column density of test particles on the line of sight between the central star and observer was computed during the simulations. Then the column density of the circumstellar dust was calculated under the assumption that the dust and gas are well mixed with a mass ratio 1 : 100. To research the influence of the disk orientation relative to the observer on the circumstellar extinction the calculations were made for four angles of inclination of the line of sight to the disk midplane and eight directions along the azimuth. The column density in the circumstellar and circumbinary disk were computed separately. The calculations have shown the periodic variations of column density can arise both in the circumstellar and circumbinary disks. The amplitude and shape of the variation strongly depend on the parameters of the simulated system (eccentricity and inclination of the orbit, the mass ratio of the companion and star) and its orientation in space. The results of our simulations can be used to explain the cyclic variation of the brightness of young UX Ori type stars.

Keywords: *hydrodynamics, circumstellar extinction, UX Ori stars, cyclic activity*

1 Introduction

Many young stars are surrounded by circumstellar gas-dust disks during the evolution of which planetary systems are born. Circumstantial evidence for their existence was obtained back in the late 1980s, before the beginning of the epoch of spaceborne and large ground-based telescopes. These were the observations of a high linear polarization in UX Ori stars during deep photometric minima that were interpreted as the influence of radiation scattered in the circumstellar disks of these stars (see, e.g., Grinin et al. 1988). The photometric and polarimetric cycles observed in some of these stars and caused by periodic circumstellar extinction variations suggested the existence of stable large-scale structures in their protoplanetary disks (see, e.g., Rostopchina et al. 2007).

Direct observations of the protoplanetary disks in various spectral regions (see, e.g., Padgett et al. 1999; Grady et al. 2005; Kalas et al. 2005; Mathews et al. 2012; Mayama et al. 2012; Kennedy et al. 2012) allowed their inclinations relative to the plane of the sky to be determined: some disks were observed nearly edge-on (see, e.g., Burrows et al. 1995; McCaughrean & O'dell 1996; Stapelfeldt et al. 1998; Stahler 2000). A number of objects were observed at a small angle to the plane of the sky, pole-on (see, e.g., Grady et al. 2000, 2001; Krist et al. 2000; Clampin et al. 2003). As the accuracy of observations increased, large-scale structures came to be identified in the disk images: spiral arms (Grady et al. 2001; Hashimoto et al. 2011; Christiaens et al. 2014; Takakuwa et al. 2014), ring-shaped gaps (Weinberger et al. 1999; ALMA Partnership et al. 2015), bright rings (Kalas et al. 2005), matter-free central cavities (Mathews et al. 2012; Mayama et al. 2012), vertical warps (Burrows et al. 1995; Heap et al. 2000), and density clumps (Greaves et al. 1998). The formation of such structures can be a consequence of the strong perturbations produced by the orbital motion of the components in young binary and multiple systems or massive planets.

The study of such processes stimulated the numerical simulations of hydrodynamic flows in the protoplanetary disks of young stars with companions. Three-dimensional (3D) hydrodynamic simulations were performed by Artymowicz (1996); Bate & Bonnell (1997); Larwood & Papaloizou (1997); Sotnikova & Grinin (2007) using the SPH (smoothed particle hydrodynamics) method. Finite-difference schemes were used in simulating binary systems by Günther & Kley (2002); Ochi et al. (2005); Hanawa et al. (2010) in the two-dimensional (2D) approximation and by Kaigorodov et al. (2010) in their 3D calculations. The gas flow structure in the circumstellar disk of a binary system was described in the above papers. The circumbinary (CB) disk of the binary system is separated from the circumstellar disks of its components by a matter-free cavity. Density waves and shocks arise at the inner boundary of the CB disk. The spiral streams of matter (originating in the CB disk) flow toward the circumstellar disks of the binary components, contributing to the accretion activity of the stars. A bridge is formed between the accretion disks of the companions through which matter from the disk of the less massive companion is transferred to the more massive one at the times of their approach at pericenter (Fateeva et al. 2011).

It should be noted that the hydrodynamic processes in the protoplanetary disks of binary stars and in the models of accretion disks around binary supermassive black holes in the nuclei of galaxies are very similar (see, e.g., MacFadyen & Milosavljević 2008; Cuadra et al. 2009; Nixon et al. 2013; D'Orazio et al. 2013; Farris et al. 2014; Gold et al. 2014; Shi & Krolik 2015; Muñoz & Lai 2016).

Spiral waves in disks can also arise when a circumstellar gas disk interacts with a planet (Lubow & Ogilvie 1998; Nelson 2000; Kley & Nelson 2008; Paardekooper et al. 2008; Marzari et al. 2009, 2012; Picogna & Marzari 2013). The formulas describing the shape of the spiral arms in such a case were proposed by Rafikov (2002) and Muto et al. (2012). In models with a planet a matter-free ring is formed (near the planet's orbit) instead of the central cavity (de Val-Borro et al. 2007). If the planet's orbit is inclined relative to the disk plane, then a vertical warp is formed in its central parts (Mouillet et al. 1997; Larwood & Papaloizou 1997; Papaloizou & Terquem 1995; Grinin et al. 2010; Demidova & Sotnikova 2013; Xiang-Gruess & Papaloizou 2013).

β Pic and CQ Tau are examples of the binary systems in which the inner parts of the disks are inclined relative to the periphery (Eisner et al. 2004; Doucet et al. 2006; Chapillon et al. 2008). The planet itself whose orbital inclination does not coincide with the disk midplane has recently been detected around the star β Pic (Lagrange et al. 2009; Chauvin et al. 2012). It should be noted that the circumstellar disk of β Pic is a debris disk that contains almost no gas. The existence of a planet in an orbit inclined to the disk in this case suggests that planets can remain for a long time in noncoplanar orbits during the evolution of the protoplanetary disk. In several cases, the perturbations by a third body located outside the disk should be taken into account to explain the observed eclipses in close binary systems surrounded by a circumbinary disk (for the simulations of unusual eclipses in the young object KH15D, see, e.g., Winn et al. 2004; Chiang & Murray-Clay 2004).

In most cases, in theoretical works the physical processes occurring in protoplanetary disks were described and the structure of the flows and inhomogeneities were investigated. A qualitative comparison of the theoretical calculations with the observed images was then made. Occasionally, simple schematic models that were not based on hydrodynamic calculations were used to calculate the asymmetry in disk images (Flaherty & Muzerolle 2010). Our works (Demidova & Grinin 2014; Ruge et al. 2015) differ in that we obtained the theoretical images of protoplanetary disks in the infrared and submillimeter spectral ranges based on the hydrodynamic models computed by the SPH method.

The perturbations in the disk produced by the motion of the companion in its orbit can also manifest themselves as circumstellar extinction variations when such systems are observed edge-on or at a small angle to the disk plane (Sotnikova & Grinin 2007; Demidova et al. 2010b,a; Grinin et al. 2010). A similar study has recently been performed by Terquem et al. (2015) based on a 2D model.

In our previous papers we performed 3D hydrodynamic computations using the SPH algorithm with constant softening length and time step. We used the code developed by Sotnikova (1996) for the investigation of interacting galaxies and modified for the simulations of protoplanetary disks (Sotnikova & Grinin 2007). During our computations we calculated the column density of circumstellar dust as a function of orbital phase at fixed azimuth and inclination of the line of sight to the disk plane. This allowed us to investigate the influence of various structures in the disk matter on the circumstellar extinction variations and light curves of UX Ori stars, i.e., young objects whose circumstellar disks are inclined at a small angle to the line of sight (Grinin et al. 1991; Kreplin et al. 2013, 2016).

In this paper we continue to investigate the perturbations in protoplanetary disks and their influence on the circumstellar extinction using the SPH algorithm with a variable softening length and an individual time step. This allows the accuracy of hydrodynamic calculations in the inner disk regions to be increased significantly.

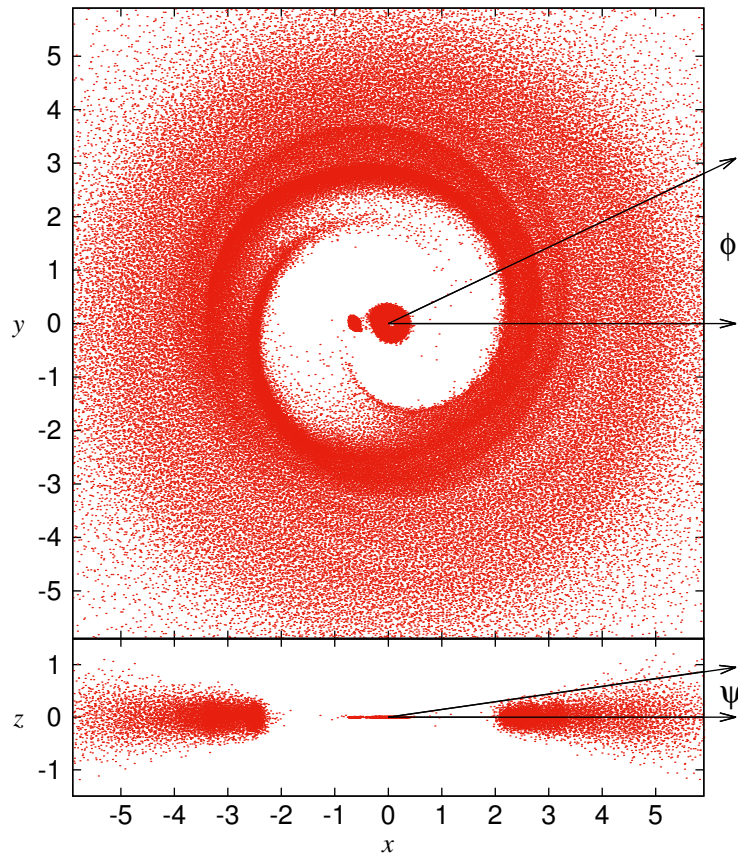


Figure 1: Distribution of matter in the disk after 20 revolutions of the companion: a pole-on view (top) and a section along the x axis (bottom). The model: $q = 0.1$, $e = 0.3$, $\theta = 0^\circ$. The distances along the axes are in units of the semimajor axis of the companion's orbit.

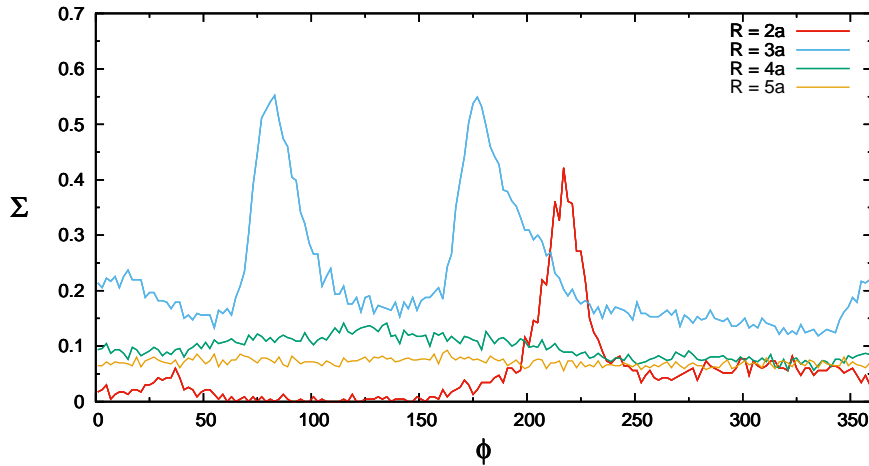


Figure 2: Surface density ($g \cdot cm^{-2}$) versus azimuth ($\phi, ^\circ$) for a given radius: $R = 2a$ (red line), $3a$ (blue line), $4a$ (green line), and $5a$ (orange line). The model: $q = 0.1, e = 0.3, \theta = 5^\circ$ after 20 revolutions of the companion.

2 The model and method

We consider the model of a gas-dust disk in which embedded two objects : a primary star with mass M_1 and a companion with mass M_2 . A component of a binary system, a substellar companion, or a giant planet can be the companion. The main parameters of the problem are the companion-to-star mass ratio $q = M_2 : M_1$, the orbital eccentricity of the companion e , and the orbital inclination of the companion to the disk plane θ (Fig. 1).

The disk mass is assumed to be small compared to the masses of the star and its companion. In this case, the disk self-gravity exerts no strong effect on the motion of the components. Therefore, we neglected this effect to reduce the computational time. The computations were performed in the isothermal approximation. Using this approximation is justified by the fact that the main source of periodic circumstellar extinction perturbations is a comparatively small (in extent) region of the CB disk near its inner boundary (Demidova et al. 2010b,a; Grinin et al. 2010). Given these assumptions, the system of hydrodynamic equations includes the continuity equation, the equation of motion, and the equation of state of an ideal gas for the isothermal case.

To numerically solve this system of equations, we use the SPH method (Lucy 1977; Gingold & Monaghan 1977), which forms the basis for the Gadget-2 code (Springel et al. 2001; Springel 2005). This code was developed for cosmological simulations. We modified this code and applied it to the computations of hydrodynamic flows in the models described above. A detailed description of the modified code is presented in Demidova (2016).

By analogy with the work of Artymowicz (1996), we specified the surface density distribution at the initial time by the law $\Sigma(r) \approx r^{-1}$; the particles were distributed in height according to a barometric law with a relative disk half-thickness $\delta = z/r = 0.1$. The Shakura-Sunyaev viscosity parameter was $\alpha_{ss} = 0.03$. The diffusion time for the surface density evolution at the distance of the companion's semimajor axis is estimated to be $t_\nu \approx 1.8 \cdot 10^4$ yr. The protoplanetary gas disk was simulated with $2.5 \cdot 10^5$ test particles that were placed at the initial time in a region of radius $R_d = 6a$, where a is the semimajor axis of the companion's orbit. At the same time, we considered a free outer boundary: the particles that went beyond $2R_d$ were deemed to have left the system and were excluded from our computations.

The test particle mass was specified to be $m_d = 10^{25}$ g, which corresponds to an accretion rate of $10^{-7} M_\odot yr^{-1}$, while the mass of the simulated region was $10^{-3} M_\odot$ in this case. In our previous models the test particle mass was determined as follows: the accretion rate was specified as a parameter of the problem and was compared with the accretion rate of test particles onto the binary components. The technique for calculating the accretion rate of test particles onto the star and its companion corresponds to that applied by Artymowicz (1996): in each time step the particles entering the zone whose radius $r = f \cdot R_{Roshe}$, where $f = const < 1$ and R_{Roshe} is the Roche lobe radius (see Eq. (2) from Eggleton 1983), are deemed to have been captured by the corresponding component. The value of f in our calculations was specified to be 0.05.

To estimate the mean accretion rate in our models, the number of particles N_i , accreting onto the star and its companion was summed over 10 orbital periods P . The relation between the accretion rate and test particle mass is then $\dot{M} = \frac{\sum_i N_i \cdot m_d}{10P}$. The mass of the simulated part of the disk can also be specified as a parameter of the problem. The sound speed in the disk matter corresponded to a temperature of 100 K. The relaxation time of the system was assumed to be 20 orbital periods of the companion. Our computations showed that over this time interval the distribution of matter in the system comes to a stable state and ceases to depend on the initial disk geometry, a matter-free cavity is formed in the central part of the disk.

During our simulations of hydrodynamic flows we computed the accretion rate of test particles onto the star and its companion and the column density of matter as a function of the phase of the orbital period. To estimate the influence of the disk orientation relative to the observer on the behavior of circumstellar extinction, we chose eight directions of the line of sight in azimuth (angle ϕ) and four inclinations in elevation (angle ψ) (Fig. 1). Along these directions we counted the number of particles on the line of sight between the observer and central star in a column of cross section $0.1 \times 0.1a$. The column densities for the circumstellar disk of the star and the CB disk (outside the companion’s orbit) were computed separately.

In Fig. 2 the surface density of matter at various distances R from the center of mass in a $R \pm 0.05a$ ring is plotted against the azimuthal angle ϕ . Four values were considered: $R = 2a, 3a, 4a, 5a$. The surface density is seen to be highly nonuniform in azimuth at $R = 2a$ and $3a$, but for $R = 5a$ the matter is distributed almost uniformly. Thus, a narrow layer of the disk contributes significantly to the circumstellar extinction variation, which justifies the use of the isothermal approximation for our problem. In addition, beyond $R > 5a$ the motion of the companion exerts no significant effect on the distribution of disk matter, and this allowed the computational domain to be limited to $R_d = 6a$. The orbital period of the companion was taken to be $P = 5$ yr for all models. For the adopted masses of the binary components this corresponds to the semimajor axis $a = 3.8$ AU. We disregarded the radiation from the low-mass companion when determining the photometric properties of the system.

3 Results

We computed a grid of models using the new code. The orbital eccentricity and inclination of the companion were varied within the ranges $e = 0-0.3$ and $\theta = 0-10^\circ$ (the apsidal line is perpendicular to the line of nodes). The companion-to-star mass ratio for all models was chosen to be $q = 0.1$. Our computations showed that the accuracy of gas flow simulations in the central regions of protoplanetary disks with companions increased considerably compared to our previous papers (Demidova et al. 2010b,a; Grinin et al. 2010). Previously unresolvable flow structures became visible: the circumstellar disks of the star and its companion and the bridge between them predicted in calculations using finite-difference schemes (Kaigorodov et al. 2010; Hanawa et al. 2010) and identified in observations (Mayama et al. 2010).

Analysis of the computed models showed that the matter dynamics in the central parts of the system agrees well with the simulations of other authors as applied to both young binary systems and binary black holes in galactic nuclei. It can be seen from Fig. 1 that a cavity filled little with matter is formed in the center of the system at a distance of the order of two semimajor axes. The shape and sizes of the cavity depend on the binary component mass ratio and eccentricity. Spiral density waves arise at the inner boundary of the CB disk (just as in Artymowicz & Lubow 1994; MacFadyen & Milosavljević 2008; D’Orazio et al. 2013). Two streams of matter that feed the disks of the companions penetrate into the central cavity from the CB disk (similar results were obtained in Artymowicz 1996; Farris et al. 2014; Muñoz & Lai 2016). The sizes of the accretion disks in our models also depend on eccentricity and closely correspond to the estimate from Artymowicz & Lubow (1994). Two-armed spiral waves (see Fig. 8 below) described previously by other authors (Nelson 2000; Kley & Nelson 2008; Picogna & Marzari 2013; Farris et al. 2014; Muñoz & Lai 2016) arise and dissipate in the inner disks of the companions. A bridge exists between the accretion disks (Kaigorodov et al. 2010; Hanawa et al. 2010; Farris et al. 2014; Muñoz & Lai 2016).

3.1 The column density in the CB disk

Figure 3 shows the behavior of the column density on the line of sight $\sigma(\phi, \psi)$ for the CB disk of a coplanar model with eccentricity $e = 0.3$. Column density oscillations with orbital phase of the companion are observed for all of the considered azimuthal angles and inclinations. However, the shape of the curve depends significantly on the disk orientation relative to the observer, because density waves arise and dissipate at certain orbital phases in the case of a noncircular orbit of the companion.

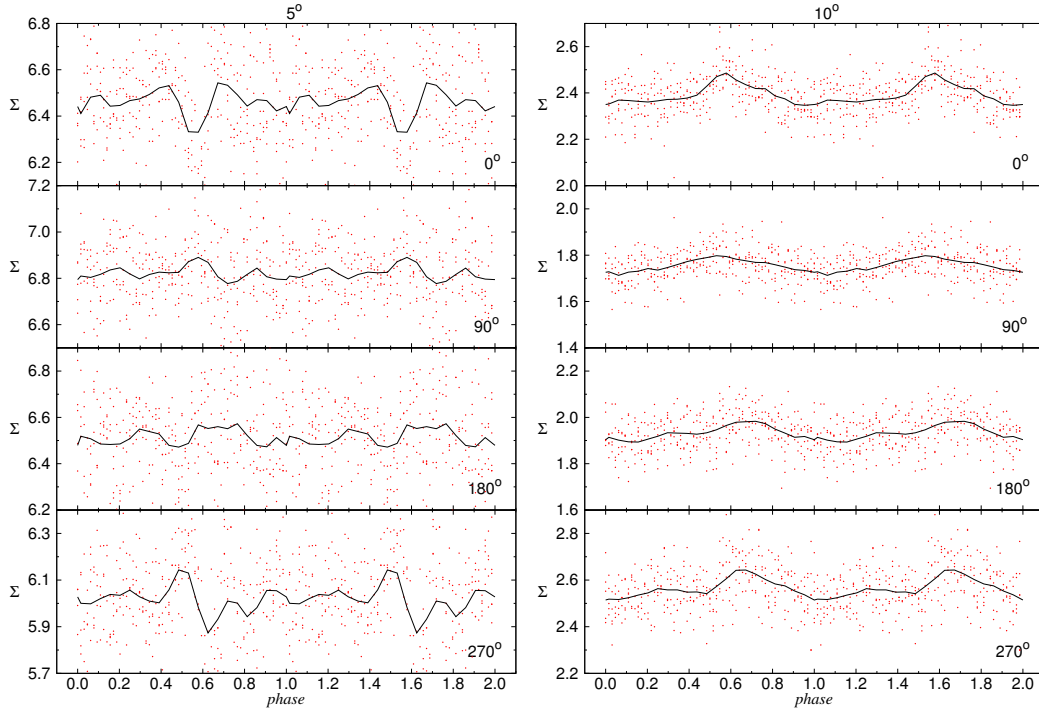


Figure 3: Column density of matter ($g \cdot cm^{-2}$) in the CB disk of the system folded with the orbital period of the companion (dots) over five periods. The solid line indicates the averaged column density (we calculated the mean for each phase of the period with a step of $1/64P$ and then performed averaging over three points by the moving average method). The model $q = 0.1, e = 0.3, \theta = 0^\circ$. The inclination of the line of sight to the disk plane ψ is 5° (left) and 10° (right). The azimuth ϕ is indicated in the lower right corner of each graph.

The results of our computations for an inclined circular model are presented in Fig. 4. Periodic column density oscillations caused by the motion of the streams and density waves at the inner disk boundary are seen for some azimuthal directions. The mean column density is also seen to depend on azimuthal angle (maximally between 270° and 0°). This is how the asymmetry of the CB disk near its inner boundary caused by the motion of the companion in an inclined orbit manifests itself the inner parts of the disk are inclined relative to its periphery. The periodic oscillations vanish for azimuthal angles of 90° and 180° due to the small amount of matter on the line of sight in these directions. The maximal column density oscillations correspond to different azimuthal angles for different inclinations: 270° and 0° for an inclination of 5° and 10° , respectively. This is how the twisting of the horizontal disk layers relative to one another manifests itself.

The amplitude of the column density oscillations increases with the orbital inclination of the companion to the disk plane (Fig. 5). However, at $\psi = 10^\circ$ and $\psi = 5^\circ$ the maximum amplitude of the column density oscillations corresponds to the same azimuthal angle of 270° . This is because in this direction the line of sight crosses the stream of matter entrained by the companion after its passage through the highest point above the disk.

On the whole, the matter dynamics in the CB disk in the computed models agrees with our previous results (Demidova et al. 2010b,a).

3.2 Computing the light curves for close binaries

A limitation of the SPH algorithm in solving the hydrodynamic equations is a small number of test particles compared to a real gas. Therefore, the test particles have a large mass. As a result, a single particle can contribute significantly to the circumstellar extinction, which can lead to large fluctuations when constructing the light curves. Therefore, to simulate the light curves, we passed from a discrete distribution of particles

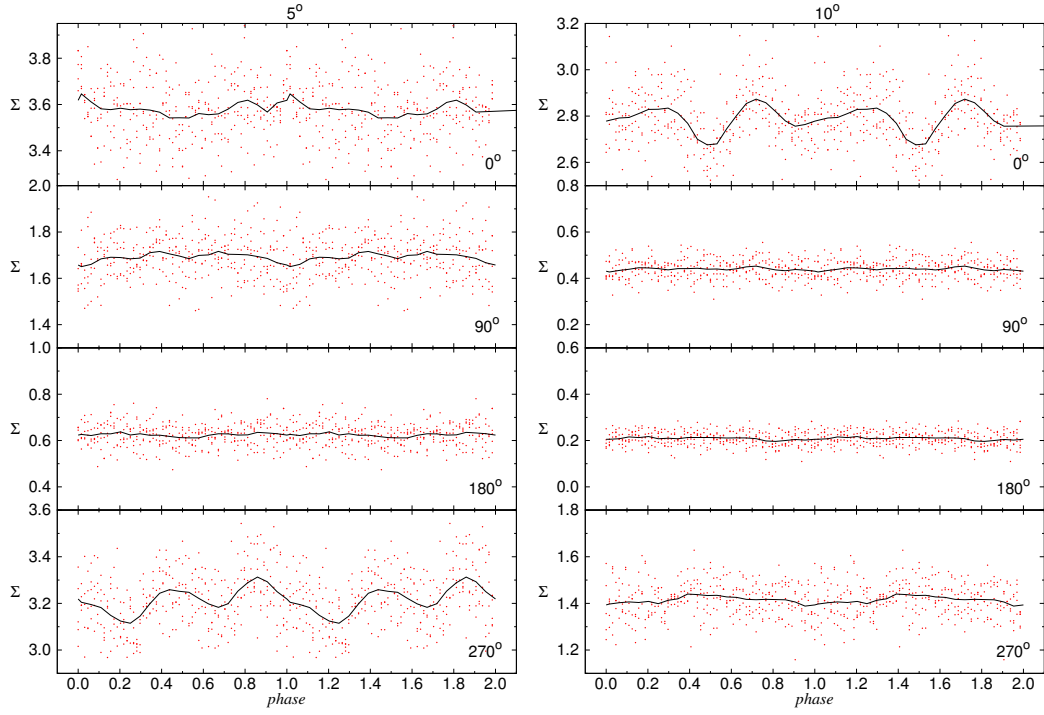


Figure 4: Same as Fig. 3, for the model $q = 0.1$, $e = 0$, $\theta = 5^\circ$.

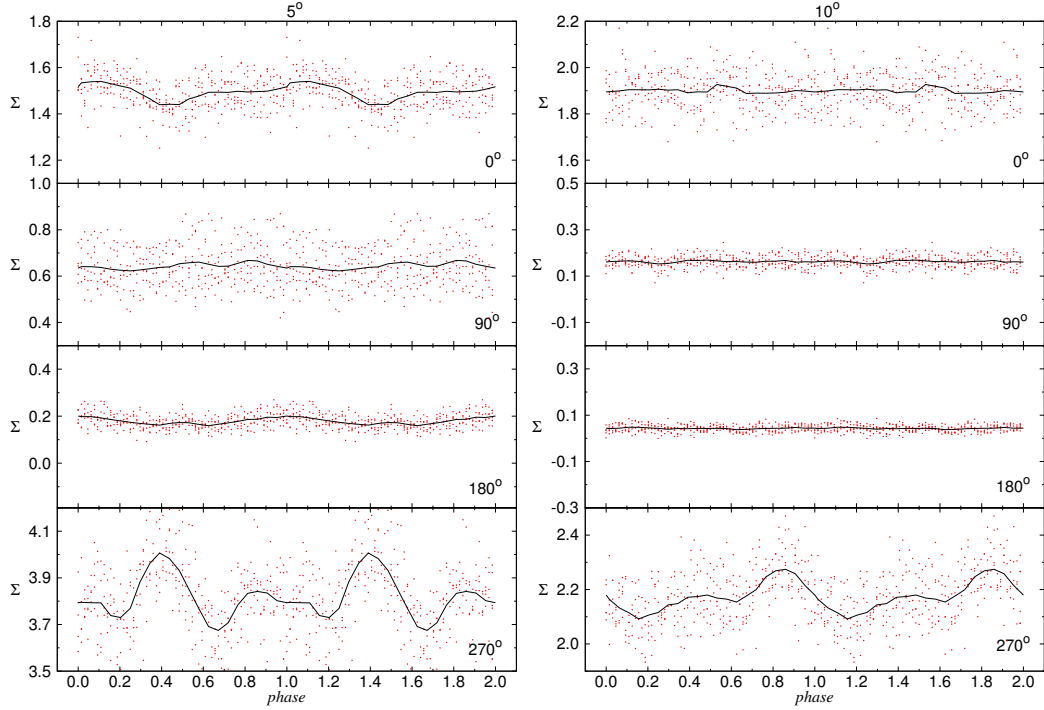


Figure 5: Same as Fig. 3, for the model $q = 0.1$, $e = 0$, $\theta = 10^\circ$.

in height z to a continuous density distribution described by a barometric law¹:

$$\rho(x, y, z) = \rho_0(x, y) \cdot e^{-\left(\frac{z}{z_0}\right)^2}. \quad (1)$$

¹A similar approach was used by Terquem et al. (2015)

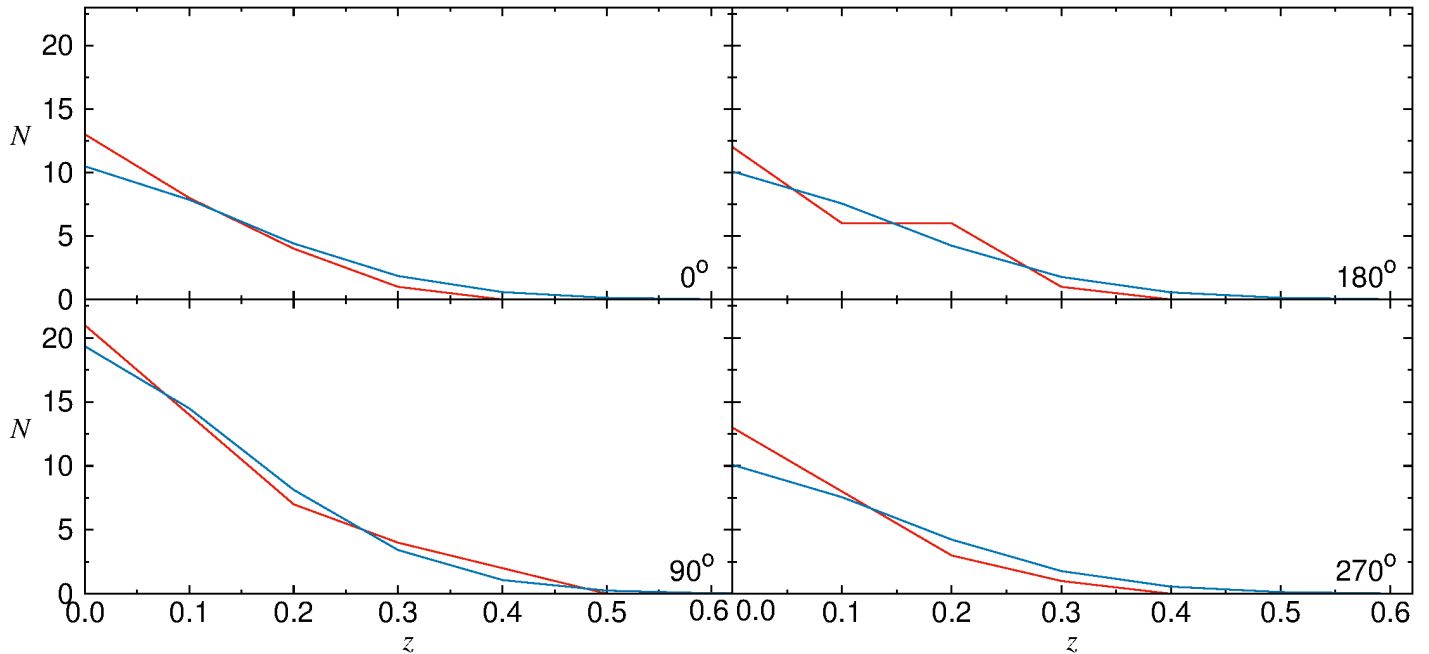


Figure 6: Distributions of test particles with height above the disk plane derived from our hydrodynamic calculations (red line) and the barometric approximation (blue line) described by Eq. (1). The time corresponds to $20P$, the distance from the central star is $3a$, the azimuth ϕ is indicated in the lower right corner of each graph.

Here, $\rho_0(x, y)$ is the density of matter in the disk plane ($z = 0$), the values of x , y , and z are measured from the system's center of mass. The disk half-thickness is defined by the relation $z_0 = \frac{V_s}{V_\phi(r)}r$, where V_s is the sound speed in the matter specified as a parameter of the problem, and $V_\phi(r)$ is the circular Keplerian speed (Shakura & Sunyaev 1973). The sound speed was assumed to be $V_s = 0.04V_\phi(a)$ (corresponding to $0.9 \text{ km} \cdot \text{s}^{-1}$ and $T = 100 \text{ K}$), by analogy with our previous papers and Artymowicz (1996).

It should be noted that the sound speed characterizes the disk viscosity and half-thickness. A decrease in V_s leads to a disk flattening (see Fig. 1 from Sotnikova & Grinin 2007) and, as a consequence, to a decrease in the optical depth on the line of sight.

Integrating Eq. (1) over z within the limit $z_1 = 0$ and $z_2 = \infty$, we obtain

$$\rho_0(x, y) = \frac{2\Sigma(x, y)}{z_0(x, y)\sqrt{\pi}}. \quad (2)$$

The values of $\Sigma(x, y)$ were derived from our hydrodynamic models as follows: the test particles were summed over the height above an elementary cell of size $S = 0.1a \times 0.1a$ (a is the semimajor axis of the companion's orbit); the number of particles was then multiplied by the mass of a single particle and divided by the cell area S . Thus, all components of Eq. (1) were determined, which allowed us to calculate the density of matter in the disk as a function of x , y , and z .

Having specified the azimuthal angle (ϕ) and inclination (ψ) of the line of sight relative to the disk plane (Fig. 1), we calculated the density of matter $\rho_i(x, y, z)$ in the direction of ϕ above each cell at height $z = \sqrt{x^2 + y^2} \cdot \tan \psi$. We then determined the column density on the line of sight $\sigma(\phi, \psi)$ and the optical depth in this direction $\tau(\phi, \psi) = \kappa \cdot \sigma(\phi, \psi)$, where κ is the opacity (in our calculations we took $\kappa = 200 \text{ cm}^2 \cdot \text{g}^{-1}$, which corresponds to Johnson's V photometric band (see Natta & Whitney 2000). The attenuation of starlight as a result of its absorption and scattering by circumstellar dust was defined by the formula $\Delta m(\phi, \psi) = -2.5 \log e^{-\tau(\phi, \psi)} = 1.085\tau(\phi, \psi)$

To check whether it is legitimate to use the barometric approximation, we compared the distribution of particles in height derived from our hydrodynamic computations and the barometric distribution of matter (Eq. (1)) at a specific radius and for a fixed time. Figure 6 shows the height dependences of the number of particles for four azimuthal angles. Passing to the barometric approximation is seen to smooth out the

particle height distribution, while the shape of the distribution is retained. It also follows from Fig. 6 that the barometric approximation describes well the changes in the amount of matter with height at various azimuthal angles (ϕ).

For a coplanar model we computed the distribution of particles during one orbital period of the P companion at specific times with a step of $1/64P$ and obtained $\Delta m(\phi, \psi)$ for each time step using the computational procedure described above. This allowed us to construct the phase light curves of the central star as a function of the disk orientation relative to the observer (Fig. 7). Periodic brightness variations are seen on all graphs; the oscillation amplitude can reach several magnitudes even at a disk inclination of 15° to the line of sight. The computations described in this and previous sections are applicable to close binary systems ($a < 4$ AU) with a hot central star of spectral type B or A , because the inner disk in this case falls into a vast dust sublimation zone and is transparent to radiation. Since the dust sublimation zone is not that large for cool T Tauri stars of spectral types from F to M , the contribution of matter from the circumstellar disk of the primary component to the column density can be significant.

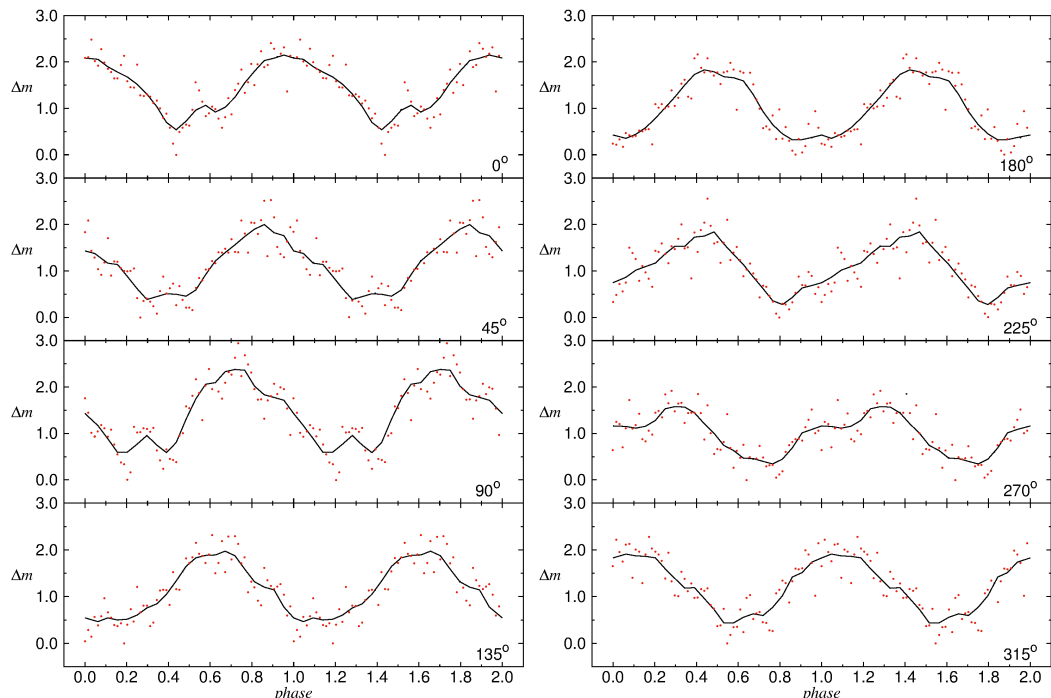


Figure 7: Phase light curves due to the extinction variations in the CB disk for the model $q = 0.1$, $e = 0.3$, $\theta = 0^\circ$, $\psi = 15^\circ$. The azimuth ϕ is indicated in the lower right corner of each graph.

3.3 Extinction in the central disk regions

A significant increase in the accuracy of calculations in the central disk region allowed us to investigate the structures emerging in the circumstellar disk of the central star. Two spiral waves produced by the tidal effect of the companion were identified. As in the papers of other authors (Nelson 2000; Kley & Nelson 2008; Picogna & Marzari 2013), in our models these structures emerge after the periastron passage by the companion and dissipate near the apastron (Fig. 8).

Figure 9 shows the behavior of the column density on the line of sight in the circumstellar disk for a coplanar model. The mean column density is seen to be independent of the azimuthal angle, i.e., the circumstellar disk is azimuthally symmetric. Column density oscillations with a period equal to the orbital one are noticeable in the curve. They are associated with the formation of two spiral waves in the circumstellar disk that emerge after the periastron passage by the companion and propagate toward the disk center and then dissipate after the apastron.

If we pass from the coplanar model to an inclined eccentric model, then the pattern of behavior of the column density changes significantly (Fig. 10). A strong dependence on the azimuthal angle appears, because

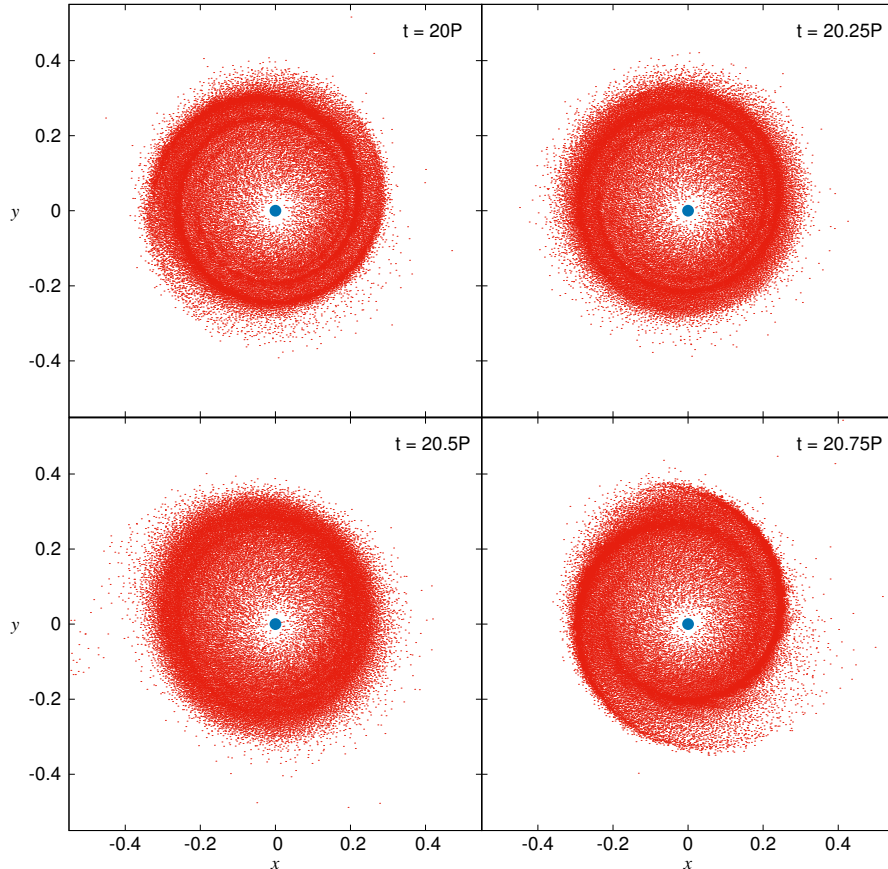


Figure 8: Pole-on view of the circumstellar disk of the primary component for various orbital phases. The model: $q = 0.1$, $e = 0.3$, $\theta = 5^\circ$. The time in units of the orbital period is indicated in the upper left corner: $t = 20P$ corresponds to the time of apastron passage by the companion. The distances along the axes are in units of the semimajor axis of the companion’s orbit.

the circumstellar disk is inclined relative to the CB disk. A trend is traceable on the graphs corresponding to azimuthal angles of 0° and 315° : the amount of matter on the line of sight increases noticeably with time. Such a behavior of the column density is caused by the precession of the circumstellar disk, which changes its orientation relative to the observer under the influence of the companion moving in an orbit inclined to the disk (this phenomenon was first considered by Larwood & Papaloizou 1997). Our computations also showed that in the model significant column density oscillations could be noticeable for some azimuthal directions at inclinations of the line of sight to the disk plane $\psi \sim 15^\circ$.

In addition, a transit of the companion’s disk along the line of sight can be observed at a “lucky” orientation of the binary system. Figure 11 shows the behavior of the column density for an inclined circular model. A narrow maximum is seen to emerge in the phase dependence of the column density at the transit time of the companion’s disk; its presence will give rise to a narrow minimum in the light curve of a young star.

Our computations showed that the perturbations in a comparatively narrow region near the inner boundary of the CB disk and in the circumstellar disk of the central star make a major contribution to the column density variations on the line of sight. It can be seen from the 2D models computed by Nelson & Marzari (2016) for the protoplanetary disk of a binary system with components similar in mass for $2 \cdot 10^6$ test particles that the structure of the system’s inner region differs noticeably for wide and close pairs. In the former case, streams of matter toward the circumstellar disks and a bridge between them are clearly seen. In closer pairs these structures are less distinct. The density of matter in these structures is lower than that at the inner boundary of the CB disk and in the disks of the binary components by several times. In our models the separation between the central star and its companion is considerably smaller than that in the paper of

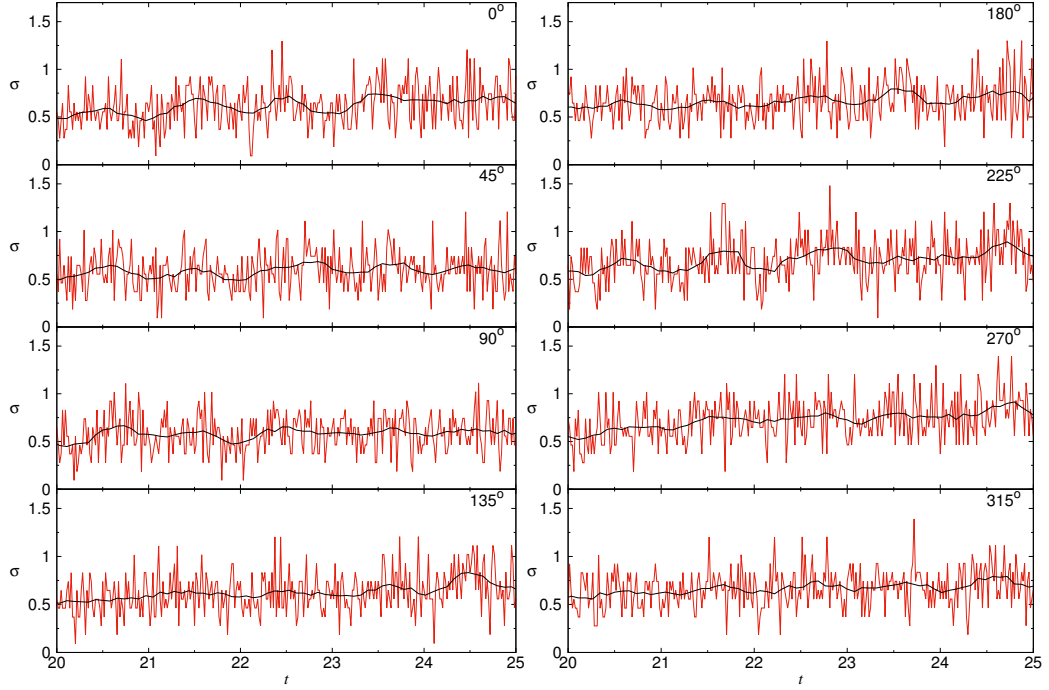


Figure 9: Column density of matter ($g \cdot cm^{-2}$) in the circumstellar disk of the primary component for the model $q = 0.1$, $e = 0.3$, $\theta = 0^\circ$, $\psi = 10^\circ$. The azimuth ϕ is indicated in the upper right corner of each graph. The time t is given in units of the orbital period of the companion.

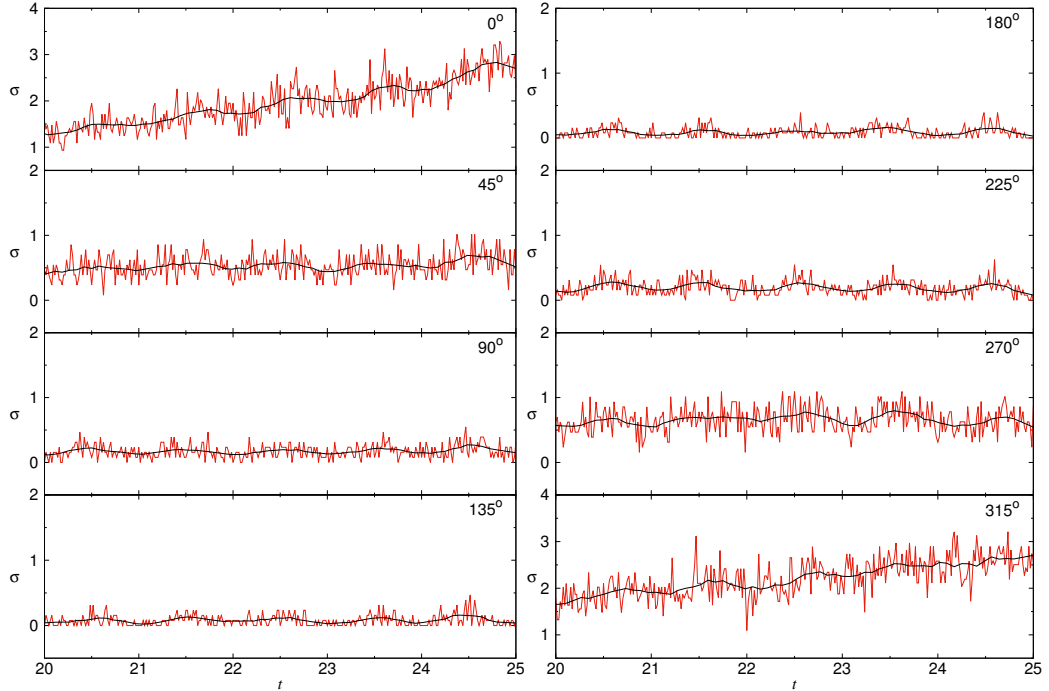


Figure 10: Same as Fig. 10, for the model $q = 0.1$, $e = 0.3$, $\theta = 5^\circ$, $\psi = 15^\circ$.

the above authors. For this reason, the bridge between the disks of the star and its companion is even less distinct (Fig. 1)).

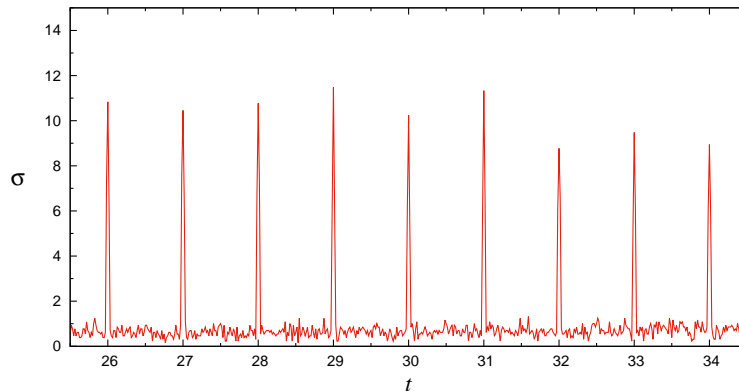


Figure 11: Column density of matter ($g \cdot cm^{-2}$) in the circumstellar disk of the primary component for the model $q = 0.1$, $e = 0$, $\theta = 5^\circ$, $\phi = 0^\circ$, $\psi = 5^\circ$.

4 Conclusions

Our computations showed that the Gadget-2 code modified by us allows the accuracy of hydrodynamic flow simulations in the central regions of the protoplanetary disks around young stars with companions to be improved significantly. This makes it possible to investigate the influence of perturbations in the disk on the photometric properties of the models under consideration and, thus, to extend the conditions for their applicability.

In our previous papers we investigated the brightness oscillations that arose in the CB disk of the star and its companion. In this case, the state of matter in the central part of the disk (within the companion’s orbit) was calculated with a low accuracy. Therefore, the results of our computations could be used for systems in which this region fell into the dust sublimation zone and did not affect the circumstellar extinction. Herbig Ae/Be stars with companions in orbits close to the stars ($a \leq 4$ AU) can be attributed to such objects. The results of this paper confirm our previous computations for the CB disk and supplement them with the studies of circumstellar extinction in the central regions.

Two-armed density waves can emerge and dissipate in the circumstellar disk of the central star with a period equal to the orbital one. This phenomenon can give rise to cyclic brightness oscillations in young stars. In addition, a transit of the companion’s disk along the line of sight can be observed at a lucky orientation of the system relative to the plane of the sky. In this case, a narrow deep minimum appears in the light curve of the central star.

Large-scale inhomogeneities, both in the CB disk of a star with a companion and in the circumstellar disk, emerge at different orbital phases for noncircular or inclined models. Therefore, to investigate the photometric properties of such systems, it is important to calculate the phase dependence of circumstellar extinction for a chosen direction rather than on the azimuthal angle.

Note that increasing the number of test particles to $2 \cdot 10^6$ in the SPH simulations of a disk around a single star can lead to disk fragmentation (Meru & Bate 2012). In addition, Nelson & Marzari (2016) showed gas fragmentation to be possible at the inner boundary of the disk around a young binary system. In this case, the fragmentation disappears if the influence of radiation from the stars of the binary system is taken into account. To investigate the influence of such effects on the light curves of UX Ori stars, we are planning to increase the number of test particles and to pass to more self-consistent models (to take into account the disk self-gravity and thermodynamics) in future papers.

Our results can be used for more detailed simulations of cyclic brightness oscillations in young stars whose disks are observed at a small angle to the line of sight (UX Ori stars) than those in previous papers. Our new, more accurate computations confirm that cyclic brightness oscillations in these stars can be markers of the presence of unresolved companions moving in the protoplanetary disks of these young stars.

Acknowledgments. This work was supported by the Russian Foundation for Basic Research (project no. 15-02-09191) and the Basic Research Program 7P of the Presidium of the Russian Academy of Sciences, the “Experimental and Theoretical Studies of Solar System Objects and Planetary Systems of Stars” Program and the Program for Support of Leading Scientific Schools (NSh-7241.2016.2).

References

- ALMA Partnership, Brogan, C. L., Pérez, L. M., et al. 2015, *ApJL*, 808, L3
- Artymowicz, P. & Lubow, S. H. 1994, *ApJ*, 421, 651
- Artymowicz, P. Lubow, S. H. 1996, *ApJ*, 467, L77
- Bate, M. R. & Bonnell, I. A. 1997, *MNRAS*, 285, 33
- Burrows, C. J., Krist, J. E., Stapelfeldt, K. R., & WFPC2 Investigation Definition Team. 1995, in *Bulletin of the American Astronomical Society*, Vol. 27, American Astronomical Society Meeting Abstracts, 1329
- Chapillon, E., Guilloteau, S., Dutrey, A., & Piétu, V. 2008, *A&A*, 488, 565
- Chauvin, G., Lagrange, A.-M., Beust, H., et al. 2012, *A&A*, 542, A41
- Chiang, E. I. & Murray-Clay, R. A. 2004, *ApJ*, 607, 913
- Christiaens, V., Casassus, S., Perez, S., van der Plas, G., & Ménard, F. 2014, *ApJL*, 785, L12
- Clampin, M., Krist, J. E., Ardila, D. R., et al. 2003, *AJ*, 126, 385
- Cuadra, J., Armitage, P. J., Alexander, R. D., & Begelman, M. C. 2009, *MNRAS*, 393, 1423
- de Val-Borro, M., Artymowicz, P., D'Angelo, G., & Peplinski, A. 2007, *A&A*, 471, 1043
- Demidova, T. V. 2016, *Astrophysics*, 59, 449
- Demidova, T. V. & Grinin, V. P. 2014, *Astron. Lett.*, 40, 334
- Demidova, T. V., Grinin, V. P., & Sotnikova, N. Y. 2010a, *Astron. Lett.*, 36, 498
- Demidova, T. V., Sotnikova, N. Y., & Grinin, V. P. 2010b, *Astron. Lett.*, 36, 422
- Demidova, T. V. Grinin, V. P. & Sotnikova, N. Y. 2013, *Astronomy Letters*, 39, 26
- D'Orazio, D. J., Haiman, Z., & MacFadyen, A. 2013, *MNRAS*, 436, 2997
- Doucet, C., Pantin, E., Lagage, P. O., & Dullemond, C. P. 2006, *A&A*, 460, 117
- Eggleton, P. P. 1983, *ApJ*, 268, 368
- Eisner, J. A., Lane, B. F., Hillenbrand, L. A., Akeson, R. L., & Sargent, A. I. 2004, *ApJ*, 613, 1049
- Farris, B. D., Duffell, P., MacFadyen, A. I., & Haiman, Z. 2014, *ApJ*, 783, 134
- Fateeva, A. M., Bisikalo, D. V., Kaygorodov, P. V., & Sytov, A. Y. 2011, *Astrophys. Space Sci.*, 335, 125
- Flaherty, K. M. & Muzerolle, J. 2010, *ApJ*, 719, 1733
- Gingold, R. A. & Monaghan, J. J. 1977, *MNRAS*, 181, 375
- Gold, R., Paschalidis, V., Etienne, Z. B., Shapiro, S. L., & Pfeiffer, H. P. 2014, *Phys. Rev. D*, 89, 064060
- Grady, C. A., Devine, D., Woodgate, B., et al. 2000, *ApJ*, 544, 895
- Grady, C. A., Polomski, E. F., Henning, T., et al. 2001, *AJ*, 122, 3396
- Grady, C. A., Woodgate, B. E., Bowers, C. W., et al. 2005, *ApJ*, 630, 958
- Greaves, J. S., Holland, W. S., Moriarty-Schieven, G., et al. 1998, *ApJL*, 506, L133
- Grinin, V. P., Demidova, T. V., & Sotnikova, N. Y. 2010, *Astron. Lett.*, 36, 808

- Grinin, V. P., Kiselev, N. N., Chernova, G. P., Minikulov, N. K., & Voshchinnikov, N. V. 1991, *Astrophys. Space Sci.*, 186, 283
- Grinin, V. P., Kiselev, N. N., Minikulov, N. K., & Chernova, G. P. 1988, *Sov. Astron. Lett.*, 14, 219
- Günther, R. & Kley, W. 2002, *A&A*, 387, 550
- Hanawa, T., Ochi, Y., & Ando, K. 2010, *ApJ*, 708, 485
- Hashimoto, J., Tamura, M., Muto, T., et al. 2011, *ApJ*, 729, L17
- Heap, S. R., Lindler, D. J., Lanz, T. M., et al. 2000, *ApJ*, 539, 435
- Kaigorodov, P. V., Bisikalo, D. V., Fateeva, A. M., & Sytov, A. Y. 2010, *Astron. Rep.*, 54, 1078
- Kalas, P., Graham, J. R., & Clampin, M. 2005, *Nature*, 435, 1067
- Kennedy, G. M., Wyatt, M. C., Sibthorpe, B., et al. 2012, *MNRAS*, 421, 2264
- Kley, W. & Nelson, R. P. 2008, *A&A*, 486, 617
- Kreplin, A., Madlener, D., Chen, L., et al. 2016, *A&A*, 590, A96
- Kreplin, A., Weigelt, G., Kraus, S., et al. 2013, *A&A*, 551, A21
- Krist, J. E., Stapelfeldt, K. R., Ménard, F., Padgett, D. L., & Burrows, C. J. 2000, *ApJ*, 538, 793
- Lagrange, A.-M., Gratadour, D., Chauvin, G., et al. 2009, *A&A*, 493, L21
- Larwood, J. D. & Papaloizou, J. C. B. 1997, *MNRAS*, 285, 288
- Lubow, S. H. & Ogilvie, G. I. 1998, *ApJ*, 504, 983
- Lucy, L. B. 1977, *AJ*, 82, 1013
- MacFadyen, A. I. & Milosavljević, M. 2008, *ApJ*, 672, 83
- Marzari, F., Baruteau, C., Scholl, H., & Thebault, P. 2012, *A&A*, 539, A98
- Marzari, F., Scholl, H., Thébault, P., & Baruteau, C. 2009, *A&A*, 508, 1493
- Mathews, G. S., Williams, J. P., & Ménard, F. 2012, *ApJ*, 753, 59
- Mayama, S., Hashimoto, J., Muto, T., et al. 2012, *ApJL*, 760, L26
- Mayama, S., Tamura, M., Hanawa, T., et al. 2010, *Science*, 327, 306
- McCaughrean, M. J. & O'dell, C. R. 1996, *AJ*, 111, 1977
- Meru, F. & Bate, M. R. 2012, *MNRAS*, 427, 2022
- Mouillet, D., Larwood, J. D., Papaloizou, J. C. B., & Lagrange, A. M. 1997, *MNRAS*, 292, 896
- Muñoz, D. J. & Lai, D. 2016, *ApJ*, 827, 43
- Muto, T., Grady, C. A., Hashimoto, J., et al. 2012, *ApJ*, 748, L22
- Natta, A. & Whitney, B. A. 2000, *A&A*, 364, 633
- Nelson, A. F. 2000, *ApJL*, 537, L65
- Nelson, A. F. & Marzari, F. 2016, *ApJ*, 827, 93
- Nixon, C., King, A., & Price, D. 2013, *MNRAS*, 434, 1946
- Ochi, Y., Sugimoto, K., & Hanawa, T. 2005, *ApJ*, 623, 922
- Paardekooper, S.-J., Thébault, P., & Mellema, G. 2008, *MNRAS*, 386, 973

Padgett, D. L., Brandner, W., Stapelfeldt, K. R., et al. 1999, *AJ*, 117, 1490

Papaloizou, J. C. B. & Terquem, C. 1995, *MNRAS*, 274, 987

Picogna, G. & Marzari, F. 2013, *A&A*, 556, A148

Rafikov, R. R. 2002, *ApJ*, 569, 997

Rostopchina, A. N., Grinin, V. P., Shakhovskoi, D. N., Lomach, A. A., & Minikulov, N. K. 2007, *Astron. Rep.*, 51, 55

Ruge, J. P., Wolf, S., Demidova, T., & Grinin, V. 2015, *A&A*, 579, A110

Shakura, N. I. & Sunyaev, R. A. 1973, *A&A*, 24, 337

Shi, J.-M. & Krolik, J. H. 2015, *ApJ*, 807, 131

Sotnikova, N. Y. 1996, *Astrophysics*, 39, 141

Sotnikova, N. Y. & Grinin, V. P. 2007, *Astron. Lett.*, 33, 594

Springel, V. 2005, *MNRAS*, 364, 1105

Springel, V., Yoshida, N., & White, S. D. M. 2001, *New Astron.*, 6, 79

Stahler, S. W. 2000, in *ESA Special Publication*, Vol. 445, *Star Formation from the Small to the Large Scale*, ed. F. Favata, A. Kaas, & A. Wilson, 133

Stapelfeldt, K. R., Krist, J. E., Ménard, F., et al. 1998, *ApJL*, 502, L65

Takakuwa, S., Saito, M., Saigo, K., et al. 2014, *ApJ*, 796, 1

Terquem, C., Sørensen-Clark, P. M., & Bouvier, J. 2015, *MNRAS*, 454, 3472

Weinberger, A. J., Becklin, E. E., Schneider, G., et al. 1999, *ApJL*, 525, L53

Winn, J. N., Holman, M. J., Johnson, J. A., Stanek, K. Z., & Garnavich, P. M. 2004, *ApJL*, 603, L45

Xiang-Gruess, M. & Papaloizou, J. C. B. 2013, *MNRAS*, 431, 1320